Supporting Online Material

Section A: Comparison between mass spectrometry and laser spectroscopy δD and $\delta^{18}O$ measurements

Comparison of the stable isotope ratios of a batch of samples (n = 48) measured by mass spectrometery and by laser spectroscopy identified offsets between the datasets (Fig. S1) similar those reported by Sturm et al. (2010). The offsets between the δD and $\delta^{18}O$ values produced a significant offset between the calculated values of d-excess (Fig. S2). For several samples tested, the difference between the d-excess derived from the GVI mass spectrometer and that derived from the LGR Liquid-Water Isotope Analyser data is greater than the analytical uncertainty. Therefore, the δD and $\delta^{18}O$ values measured on the LGR Liquid-Water Isotope Analyser (δD_{laser}) were corrected to make them comparable to the GVI mass spectrometer values ($\delta D_{mass\ spec.\ equiv.}$) using the least squares linear relationships established by analysing samples on both instruments (e.g., Fig. S1).

$$\delta D_{mass\ spec.\ equiv.} = (1.013 * \delta D_{laser}) + 1.746$$

$$\delta^{18}O_{mass\ spec.\ equiv.} = (0.986 * \delta^{18}O_{laser}) - 0.711$$

Deuterium excess values were then calculated from the corrected δD and $\delta^{18}O$ datasets. A revised analytical uncertainty (u) for d-excess, which takes into account the errors on both instruments, is calculated as: $\sqrt{(1.3^2 + 1.7^2)} = 2.1‰$. The d-excess record of the MES ice core before and after the above corrections were applied is displayed in Figure A3.

Sturm, P. and Knohl, A.: Water vapor δ^2H and $\delta^{18}O$ measurements using off-axis integrated cavity output spectroscopy, Atmospheric Measurement Techniques, 3,67-77, 2010

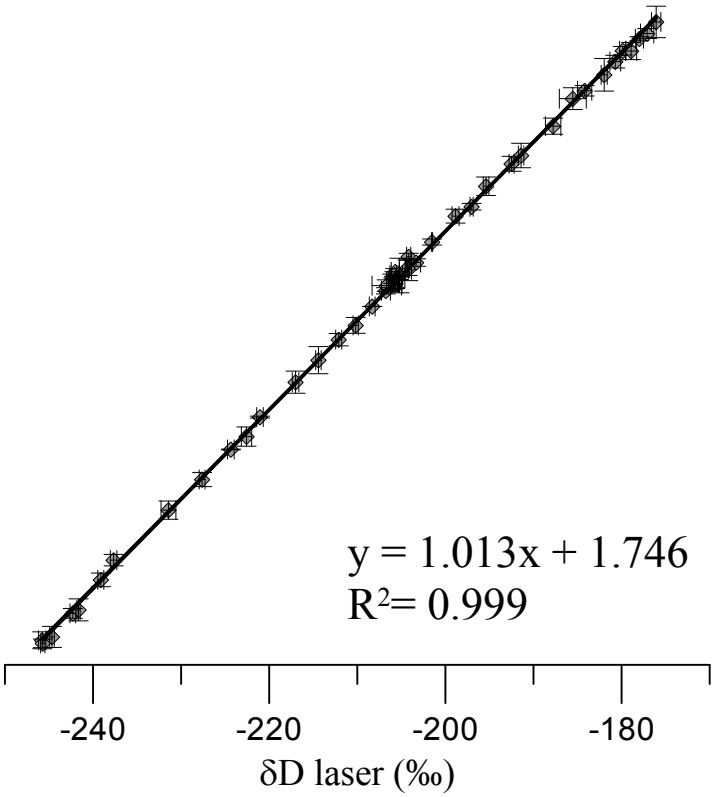

Figure S1: Linear least squares relationship between δD measured on GVI mass spectrometer and LGR Liquid-Water Isotope Analyser (Laser). Error bars are 2σ.

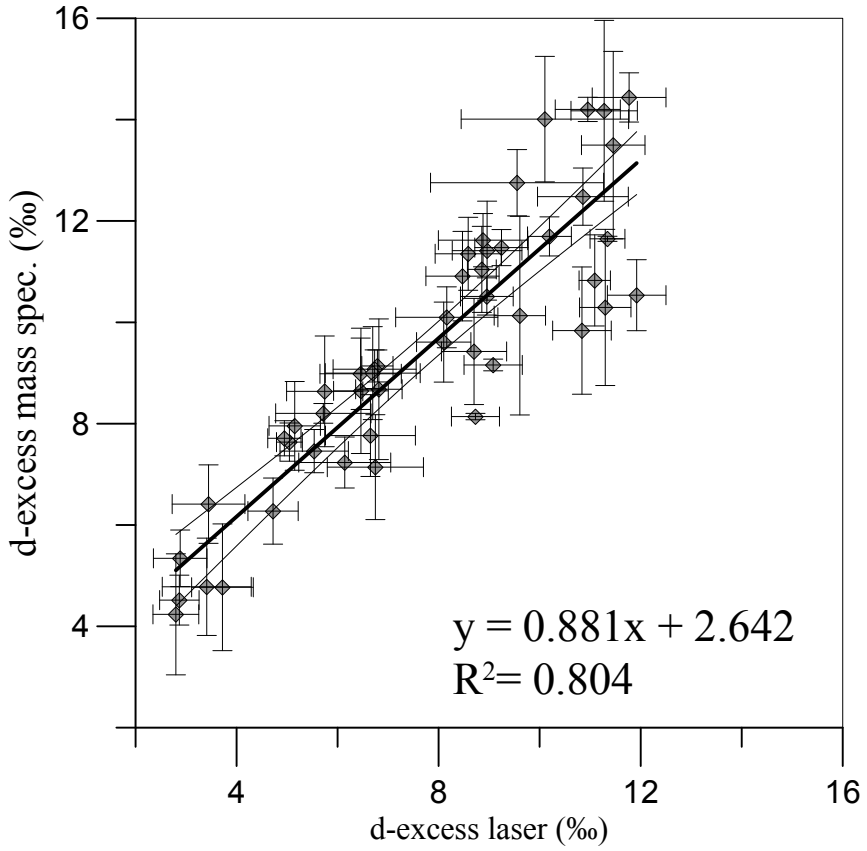

Figure S2: Linear least squares relationship between d-excess derived from $\delta^{18}O$ and δD values measured on GVI mass spectrometer and LGR Liquid-Water Isotope Analyser (Laser). Error bars are analytical uncertainty (u) ($u = \sqrt{(a^2+(8*b^2))}$, where a = precision (2 σ) on δD and b = precision (2 σ) on $\delta^{18}O$).

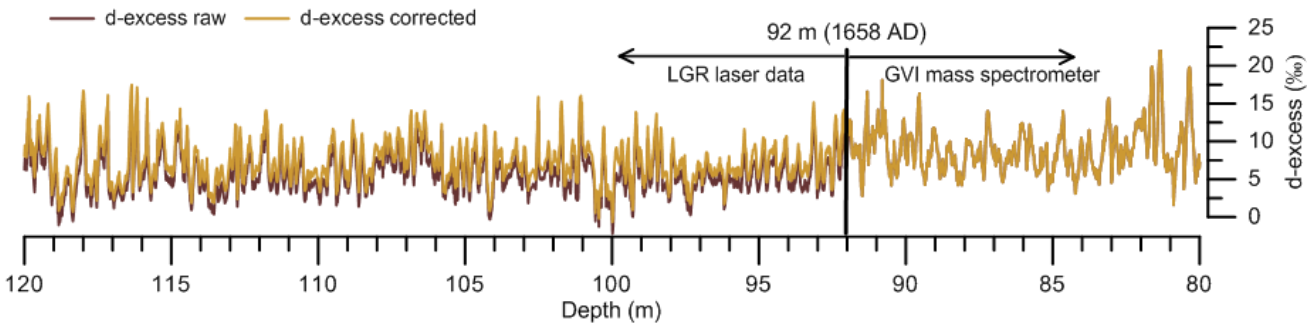

Figure S3: MES ice core d-excess record before and after a correction was applied to laser-measured data to account for the offset between the mass spectrometer and laser instruments.

Section B: ICP-MS and IC analytical methods

Procedural blank measurements were conducted on samples generated from mock ice cores of frozen ultra-pure water (> 18.2 MΩ), which were processed, melted and sampled daily by the methods described in Section 2.2. Chemical concentrations determined in procedural blanks by IC and ICP-MS are displayed in Table S1. The significant Zr and Ca concentrations recorded originate from ceramic knives used to prepare the ice core for melting. The IC Ca^{2+} blank displays additional contamination speculated to originate from elution of Ni, from the melter head disk, in a region close to Ca^{2+} on the CS-12A column (Osterberg et al., 2006). These chemical species were not considered during interpretation.

The detection limits achieved on the IC and ICP-MS instruments are displayed in Table S1. This study employed an Agilent 7500cs Series ICP-MS whilst the majority of previous ICP-MS trace element studies conducted on Antarctic ice core samples have employed sector-field (SF) ICP-MS instruments. Detection limits from two recent SF-ICP-MS studies are displayed in Table S1 for comparison. For several elements (Ti, V, Rb, Pb and Ba) the detection limits from this study are either lower or within 1 ppt of those achieved with SF-ICP-MS.

The operating conditions of the ICP-MS are displayed in Table S2. An ASX-520 micro-volume autosampler introduced sample to the PFA Teflon nebuliser (0.2 mL min^{-1} flow rate) via a peristaltic pump. The formation of oxides in the plasma was monitored by aspiration of a 1 ppb Ce solution. Tuning parameters were adjusted to maintain the proportion of the ^{140}Ce converted to $^{140}Ce^{16}O$ at < 2%. The sampling and skimmer cones were cleaned, and the sample introduction system was circulated with 5 wt.% HNO_3 (Seastar) for 1 hr prior to each analytical session to reduce any possible memory effects from the samples of previous users.

Table S1: Procedural blank concentrations and detection limits (3σ on blank) of chemical species by ICP-MS (units are ppt = parts per trillion) and IC (units are ppb = parts per billion).

ICP-MS Element	Procedural blank	Detection limit	Detection limit Gabrielli et al. (2005)[a]	Detection limit Barbante et al. (1999)[b]
Na	1120	167		
Mg	290	5.02		
Al	560	9.72		
Ca	6890	1271		
Ti	78.5	22.5		63
V	< D.L.	0.83	0.4	3
Mn	10.9	3.22	0.3	1.8
As	< D.L.	6.73	1	
Rb	0.47	0.31	0.5	
Sr	4.50	0.31	5	
Y	0.50	0.10		
Zr	3.05	0.58		
Cs	< D.L.	0.18		
Ba	5.28	0.32	2	1.8
La	0.66	0.14		
Ce	1.42	0.19		
Pr	< D.L.	0.19		
Tl	< D.L.	0.44		
Pb	4.67	0.72		0.6
Bi	< D.L.	0.43	0.02	0.09
Th	< D.L.	0.45		
U	< D.L.	0.40	0.01	0.03

IC Ion	Procedural blank	Detection limit
Na^+	0.34	0.16
Mg^{2+}	0.66	0.51
K^+	< D.L.	0.33
Ca^{2+}	20.3	0.08
MS^-	< D.L.	0.32
Cl^-	26.6	0.76
SO_4^{2-}	12.8	0.43
NO_3^-	6.27	0.35

[a] Gabrielli, P., et al. (2005b), Trace elements in Vostok Antarctic ice during the last four climatic cycles, *Earth and Planetary Science Letters*, *234*, 249-259

[b] Barbante, C., G. Cozzi, G. Capodaglio, K. van de Velde, C. Ferrari, C. F. Boutron, and P. Cescon (1999), Trace element determination in alpine snow and ice by double focusing inductively coupled plasma mass spectrometry with microconcentric nebulization, *Journal of Analytical Atomic Spectrometry*, *14*, 1433-1438

< D. L. = below detection limit

Table S2: ICP-MS operating conditions and data acquisition parameters for the determination of selected elements in MES ice core samples

Parameter	**Setting**
Forward power	1500 W
RF matching	1.75-1.84 V
Carrier gas	1.04-1.10 L min^{-1}
Makeup gas	0 L min^{-1}
Nebulizer pump	0.12-0.16 rps
Spray chamber temperature	2 °C
Sampling depth	7 mm
Torch position	Optimised daily to maximise sensitivity
Ion lenses voltages	Optimised daily to maximise sensitivity and signal stability across mass range
Isotopes measured	^{23}Na, ^{24}Mg, ^{27}Al, ^{43}Ca, ^{47}Ti, ^{51}V, ^{55}Mn, ^{75}As, ^{85}Rb, ^{88}Sr, ^{89}Y, ^{90}Zr, ^{133}Cs, ^{138}Ba, ^{139}La, ^{140}Ce, ^{141}Pr, ^{205}Tl, ^{208}Pb, ^{209}Bi, ^{232}Th, ^{238}U
Uptake and stabilization time	50 s and 60 s
Washing time between samples	10 s H_20, 200 s 5 wt.% HNO_3 (Seastar), 220 s 1 wt.% HNO_3 (total 430 s)
Integration time	0.10 s or 0.15 s depending on element
No. of runs and scan passes	3 x 26

Section C: Dating of the ice core

Back-diffused δD and $\delta^{18}O$ records were used to pick annual layers in the ice core to 61.1 m depth. Raw and back-diffused δD records for an example section of core are displayed in Figure S4. Below 61.1m an ice flow model was used to predict the age-depth relationship (Fig. S5).

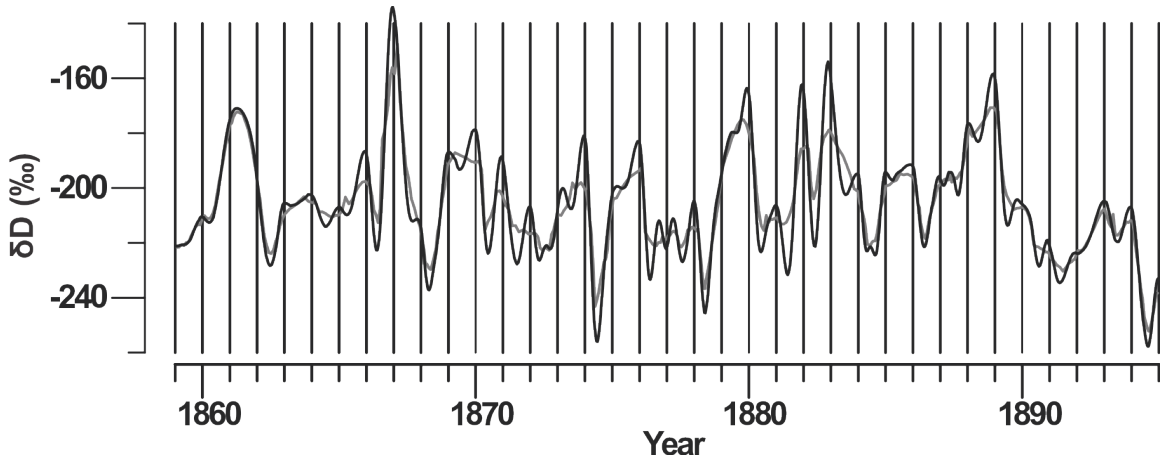

Figure S4: Raw (grey curve) and back-diffused (black) δD time series for 40–50 m depth of MES ice core. Vertical grid lines indicate the location of picked annual layers.

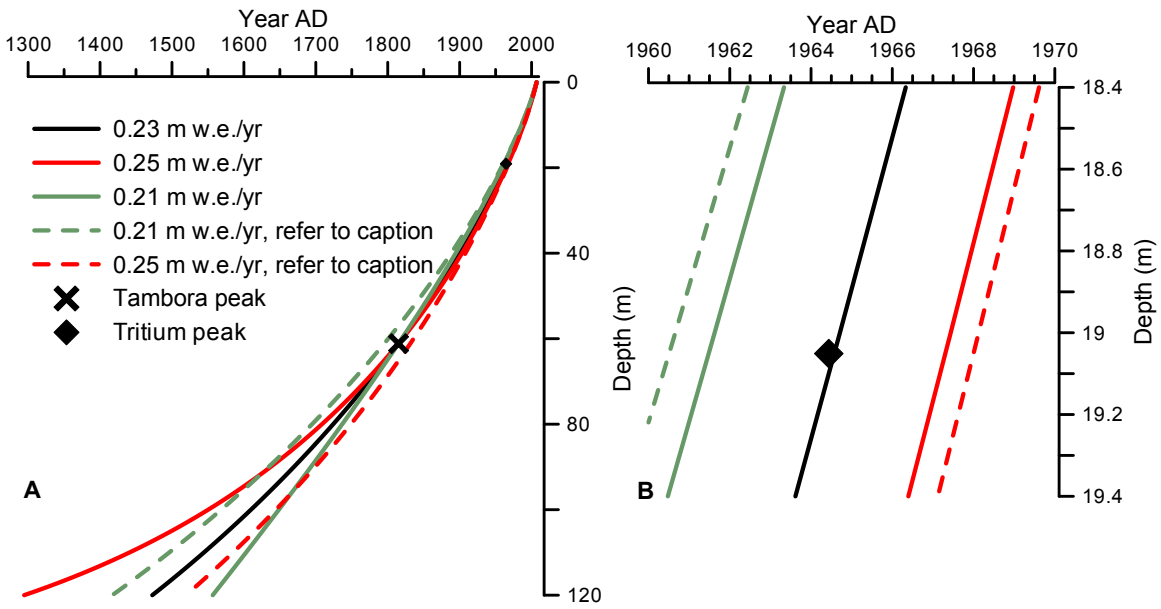

Figure S5: A) Age-depth results of the Dansgaard-Johnsen ice flow model run with three different accumulation rates. Solid lines were produced by tuning the kink-height to force the model output through the Tambora eruption. Dashed lines were produced using the same kink-height tuning as for the black line (23 m w.e. yr^{-1}) but the output was not forced to match the position of the Tambora eruption. B) Enlargement of A to correspondence of flow model results and tritium peak position. The flow parameters were not adjusted to force the model through the tritium peak for any of these runs.